**Earthquakes and Structures**, *Vol. 11, No. 6 (2016) 1077-1099*
DOI: http://dx.doi.org/10.12989/eas.2016.11.6.1077 

# Lyapunov-based Semi-active Control of Adaptive Base Isolation System employing Magnetorheological Elastomer base isolators

Xi Chen[1], Jianchun Li*[2], Yancheng Li**[2] and Xiaoyu Gu[2]

[1]*School of Electrical Engineering and Automation, Tianjin University, Tianjin City, 300072, China*
[2]*School of Civil and Environmental Engineering, University of Technology Sydney, NSW 2007, Australia*

*(Received March 16, 2016, Revised June 2, 2016, Accepted July 6, 2016)*

**Abstract.** One of the main shortcomings in the current passive base isolation system is lack of adaptability. The recent research and development of a novel adaptive seismic isolator based on magnetorheological elastomer (MRE) material has created an opportunity to add adaptability to base isolation systems for civil structures. The new MRE based base isolator is able to significantly alter its shear modulus or lateral stiffness with the applied magnetic field or electric current, which makes it a competitive candidate to develop an adaptive base isolation system. This paper aims at exploring suitable control algorithms for such adaptive base isolation system by developing a close-loop semi-active control system for a building structure equipped with MRE base isolators. The MRE base isolator is simulated by a numerical model derived from experimental characterization based on the Bouc-Wen Model, which is able to describe the force-displacement response of the device accurately. The parameters of Bouc-Wen Model such as the stiffness and the damping coefficients are described as functions of the applied current. The state-space model is built by analyzing the dynamic property of the structure embedded with MRE base isolators. A Lyapunov-based controller is designed to adaptively vary the current applied to MRE base isolator to suppress the quake-induced vibrations. The proposed control method is applied to a widely used benchmark base-isolated structure by numerical simulation. The performance of the adaptive base isolation system was evaluated through comparison with optimal passive base isolation system and a passive base isolation system with optimized base shear. It is concluded that the adaptive base isolation system with proposed Lyapunov-based semi-active control surpasses the performance of other two passive systems in protecting the civil structures under seismic events.

**Keywords:** Magnetorheological Elastomer; Adaptive Base Isolation; Semi-active control; Lyapunov-based control; Bouc-Wen model; stability

## 1. Introduction

One of the most widely implemented and accepted vibration control techniques for seismically excited structures is the passive base isolation. Base isolation isolates the structure and its contents

*Corresponding author, E-mail: Jianchun.Li@uts.edu.au
**Corresponding author, E-mail: Yancheng.li@uts.edu.au


http://www.techno-press.com/journals/eas&subpage=7 ISSN: 2092-7614 (Print), 2092-7622 (Online)

from damaging earthquakes by lengthening the fundamental periods of the structure, therefore keeps them away from the dominant period of the earthquake excitations (Hosseini and Farsangi 2012, Murase *et al.* 2013, Patil *et al.* 2016). However, such system inevitably inherits certain shortcomings of a passive system. As Tarek *et al.* (2015) pointed out that current base isolation practices with passive nature can be considered as systems with a 'limited intelligence because these structures are unable to adapt to the excitation and global structural response', and thus are characterized by a limited control capacity. They are optimally tuned to protect the structures from a specified dynamic loading, but their efficiency will not be the optimal one for other cases and other types of dynamic loadings.

To improve the adaptability of base isolation systems, semi-active control devices which are natural extensions of passive isolator devices are intensively investigated in recent years, forming a new category of base isolation system, termed as hybrid base isolation system. Hybrid base isolation systems often consist of passive base isolators with active or semi-active energy dissipation devices, such as semi-active dampers. These additional supplementary damping devices (Tarek *et al*. 2015) are to dissipate energy transmitted to the main structure due to seismic excitations. In those semi-active control applications, the adaptive systems regulate the damper behavior based on the collected information of excitation and structural response. Several comprehensive reviews can be found in Housner *et al*. (1997), Spencer *et al*. (2003), Fisco *et al.* (2011), Liu *et al.* (2009) and Fabio *et al.* (2012). It has been demonstrated that adding semi-active or active damping can significantly absorb the seismic energy in the structure. However, with passive base isolators in the system it is less effective in terms of changing the fundamental period of the building system which is the underlining principle of the base isolation system.

Li *et al*. (2013a, b) presented an adaptive laminated base isolator prototype named magnetorheological elastomer (MRE) base isolator whose elastic modulus increases monotonically with the magnetic field. The proposed MRE base isolator inherited the unique laminated structure of the traditional based isolator, with multilayer steel and MRE sheets, enabling the high axial stiffness and low lateral stiffness requirements of civil engineering applications (Li *et al.* 2015a). The experimental results showed that force increase of the new generation MRE base isolator is up to 1630% (Li *et al*. 2015b), which is suitable for semi-active control for seismically excited structures. By taking advantage of the controllable stiffness, the development of the adaptive base isolation system for civil structure becomes feasible. However, one challenge hindering such development is the development of suitable control algorithms for the adaptive base isolation system, which utilize the mechanism of the base isolation and incorporate the inherent hysteresis of the MRE base isolator. To this end, several models have been proposed to describe non-linear hysteretic behavior of MRE base isolator. Yang *et al*. (2013) developed a Bouc-Wen model to predict the force-displacement response of MRE. Li *et al.* (2013b) proposed a strain-stiffening model for the MRE base isolator which contains five model parameters, much less than that of the Bouc-Wen model. Yu *et al.* (2015a) presented an enhanced optimization algorithm based on Particle swarm optimization for parameter identification of the model as in Li *et al*. (2013b). Yu *et al*. (2014) put forward a model consisting of a hyperbolic expression and the identification of parameters was implemented by a modified artificial fish swarm algorithm. Yu *et al*. (2015b) proposed an improved LuGre friction model for MRE base isolator and proposed an improved fruit fly optimization algorithm to identify the model parameters. On the other hand, the controller design for MRE base isolation system has also been explored. Gu *et al*. (2015) developed a novel frequency control algorithm for the adaptive base isolation system to shift the fundamental frequency of the structure away from the dominant

frequency range of earthquakes. And yet, more efforts are to be made to fully take advantage of the unique features of the MRE base isolators to develop more effective base isolation techniques.

This paper will theoretically explore the development of a Lyapunov-based semi-active control for the adaptive base isolation system. To characterize the hysteretic behavior of the MRE base isolator, Bouc-Wen model is adopted in this paper for the control simulation. A Lyapunov-based controller is then designed and integrated into the state-space description of base-isolated civil structure. Comprehensive numerical investigations are undertaken to investigate the effectiveness of the adaptive base isolation system with the proposed control algorithm.

## 2. Modelling of novel adaptive MRE base isolator

The structure of the adaptive MRE base isolator is illustrated in Fig. 1. The MRE base isolator consists of several important components, that is, laminated MRE and steel core, electromagnetic coil, cylindrical steel yoke, and connecting plates at each side. The laminated structure is to maintain the high load-carrying capacity in vertical direction and low lateral stiffness in horizontal direction. Electromagnetic coil is to energize the MRE material in the core with sufficient magnetic field (Li *et al*. 2015b). Top and bottom plates are to connect the device with ground and superstructure. Under horizontal loadings, the laminated core deforms with the limit of gap between itself and the yoke. In this design, there are 25 layers of the steel sheet with thickness of 1 mm and 26 layers of MRE sheets with thickness of 1 mm being used. The cylindrical electromagnetic coil has an inner diameter of 150 mm and an outer diameter of 200 mm.

To obtain the characteristics of MRE base isolator, a series of experimental testing were carried out, shown in Fig. 2. In every test, the device was driven with a sinusoidal excitation of three different magnitudes (2, 4, and 8 mm) at a wide range of frequencies (0.1, 1, 2, and 4 Hz). The horizontal force was measured by a load cell under four different supplied currents (1, 2, 3, and 4A).

It is clearly that MRE base isolator is of hysteretic nature. Because of the numerical capacity to demonstrate all sorts of hysteresis, the Bouc-Wen model is used to describe non-linear hysteretic behavior of MRE base isolator, given by

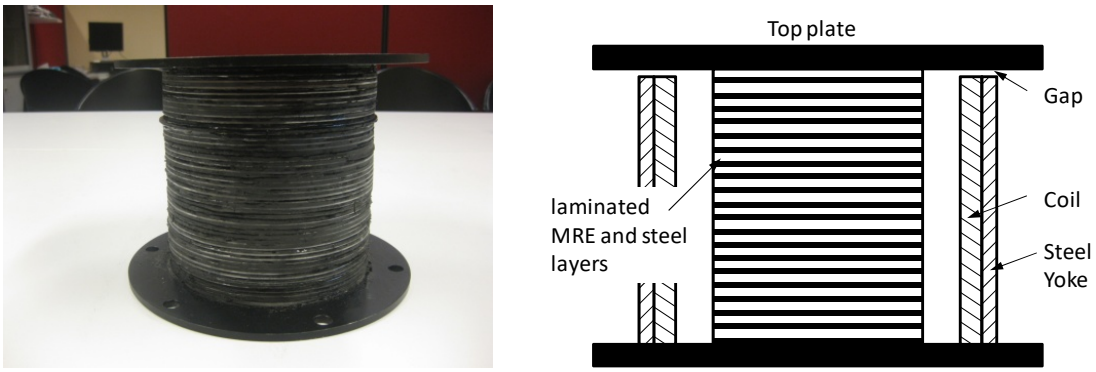


(a) The Exterior (b) Cross-section view

Fig. 1 MRE Base Isolator

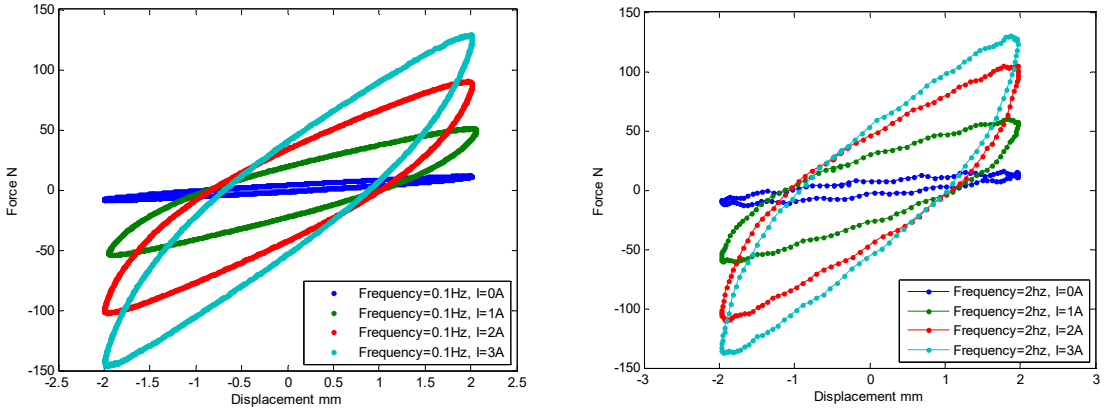


(a) Frequency=0.1 Hz (b) Frequency=2.0 Hz

Fig. 2 Force-displacement relationships of the MRE base isolator

$$\Phi(u_1,t)=\alpha k_1 u_1+c_1\dot{u}_1+(1-\alpha)k_1 Dz(t) \tag{1}$$

$$\dot{z}(t)=D^{-1}\left(\theta\,\dot{u}_1-\beta|\dot{u}_1||z|^{n-1}z-\lambda\dot{u}_1|z|^n\right) \tag{2}$$

$$k_1=k_{11}(I_0-i)+k_{10} \tag{3}$$

$$c_1=c_{11}(I_0-i)+c_{10} \tag{4}$$

where, $D$>0 is the yield constant displacement and $\alpha\in(0,1)$ is the post- to pre-yielding stiffness ratio. $z(t)$ is called evolutionary variable which is the hysteretic part defined by Eq. (2). $I_0$ is the constant current supplied for MRE when there's no earthquakes. $i$ is the control current of MRE which varies during seismic events. $\theta$, $\beta$, $\lambda$ and $n$ are non-dimensional parameters which are responsible for the shape and the size of the hysteretic loops. A detailed discussion on the above parameters can be found in Sues *et al*. (1988) and Faycal *et al.* (2007).

## 3. The design of Lyapunov-based controller

### *3.1 The state-space model of the seismically excited structure embedded with MRE*

In this study, a multi-degree-of-freedom civil structure with n floors is used for theoretical investigations, as shown in Fig. 3. Base isolation system containing MRE base isolators is installed beneath the building. The MRE base isolator is described by a Bouc-Wen model depending on the current as detailed in Section 2. $m_j$ is the concentrated mass of the floor $j$. $c_j$ and $k_j$ are the damping and stiffness coefficients between story $j$ and $j$-1, $u_j$ is the relative displacement and $\dot{u}_j$ is the relative velocity of story $j$.

The state-space model is developed for the control of the structure isolated by MRE isolators. The motion equation at floor $n$ is derived as

$$m_n\ddot{u}_n + c_n\left(\dot{u}_n - \dot{u}_{n-1}\right) + k_n\left(u_n - u_{n-1}\right) = -m_n\ddot{x}_g \tag{5}$$

By applying the same methodology, the motion equation at story $j$ ($j$=2,…,$n$-1) can be written as

$$m_j\ddot{u}_j + c_j\left(\dot{u}_j - \dot{u}_{j-1}\right) + k_j\left(u_j - u_{j-1}\right) - c_{j+1}\left(\dot{u}_{j+1} - \dot{u}_j\right) - k_{j+1}\left(u_{j+1} - u_j\right) = -m_j\ddot{x}_g \tag{6}$$

The motion equation at story 1 which is immediately above the MRE isolation system is expressed as follows

$$m_1\ddot{u}_1 - c_2\left(\dot{u}_2 - \dot{u}_1\right) - k_2\left(u_2 - u_1\right) + \Phi\left(u_1, t\right) = -m_1\ddot{x}_g \tag{7}$$

$\Phi(u_1,t)$ is defined in Eq. (1), which is the Bouc-Wen model. $x_g$ and $\dot{x}_g$ are the displacement and velocity of ground, respectively.

Substituting Eqs. (1), (2), (3), (4) into Eq. (7), the motion equation at floor 1 becomes

$$\begin{aligned} &m_1\ddot{u}_1 + \left[c_{11}\left(I_0 - i\right) + c_{10}\right]\dot{u}_1 - c_2\left(\dot{u}_2 - \dot{u}_1\right) + \alpha\left[k_{11}\left(I_0 - i\right) + k_{10}\right]u_1 \\ &- k_2\left(u_2 - u_1\right) + \left(1-\alpha\right)\left[k_{11}\left(I_0 - i\right) + k_{10}\right]Dz\left(t\right) = -m\ddot{x}_g \end{aligned} \tag{8}$$

Define the state variable $x = \left[u_1 \;\; \cdots \;\; u_n \;\; \dot{u}_1 \;\; \cdots \;\; \dot{u}_n\right]$, then Eqs. (5), (6), (7), (8) can be expressed in matrix notations and symbolically expressed as below

$$\dot{x} = Ax + b\left(x\right)i + W_{BW} + W_e \tag{9}$$

where

$$A = \begin{bmatrix} 0_n & I_n \\ -M^{-1}K_n & -M^{-1}C_n \end{bmatrix} \quad \text{and} \quad b\left(x\right) = \begin{bmatrix} 0_n \\ \dfrac{c_{11}\dot{u}_1 + \alpha k_{11}u_1}{m_1} \\ 0_{n-1} \end{bmatrix}$$

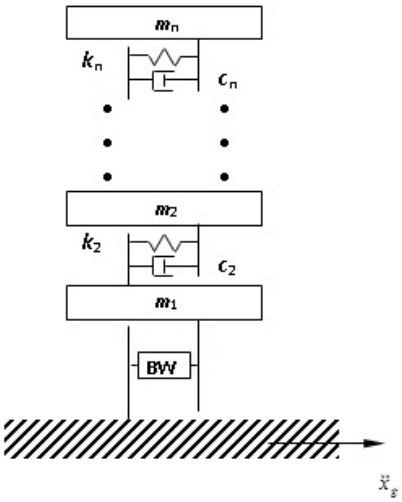


Fig. 3 Multi-degree-of-freedom (MDOF) model of structural system with MRE

$$M=\begin{bmatrix} m_1 & & & & & & \\ & m_2 & & & & & \\ & & \ddots & & & & \\ & & & m_j & & & \\ & & & & \ddots & & \\ & & & & & m_{n-1} & \\ & & & & & & m_n \end{bmatrix}$$ is the mass matrix.

$$K_n=\begin{bmatrix} \alpha(k_{11}I_0+k_{10})+k_2 & -k_2 & \cdots & 0 & \cdots & 0 & 0 \\ -k_2 & k_2+k_3 & \cdots & 0 & \cdots & 0 & 0 \\ \vdots & \vdots & \ddots & \vdots & \cdots & \vdots & \vdots \\ 0 & 0 & \cdots & k_j+k_{j+1} & \cdots & 0 & 0 \\ \vdots & \vdots & \cdots & \vdots & \ddots & \vdots & \vdots \\ 0 & 0 & \cdots & 0 & \cdots & k_{n-1}+k_n & -k_n \\ 0 & 0 & \cdots & 0 & \cdots & -k_n & k_n \end{bmatrix}\in R^{n\times n}$$

is the stiffness matrix.

$$C_n=\begin{bmatrix} c_{11}I_0+c_{10}+c_2 & -c_2 & \cdots & 0 & \cdots & 0 & 0 \\ -c_2 & c_2+c_3 & \cdots & 0 & \cdots & 0 & 0 \\ \vdots & \vdots & \ddots & \vdots & \cdots & \vdots & \vdots \\ 0 & 0 & \cdots & c_i+c_{i+1} & \cdots & 0 & 0 \\ \vdots & \vdots & \cdots & \vdots & \ddots & \vdots & \vdots \\ 0 & 0 & \cdots & 0 & \cdots & c_{n-1}+c_n & -c_n \\ 0 & 0 & \cdots & 0 & \cdots & -c_n & c_n \end{bmatrix}\in R^{n\times n}$$ is the damping matrix.

$$W_e=\begin{bmatrix} 0_n \\ -1_n \end{bmatrix}\ddot{x}_g$$

$$1_n=\begin{bmatrix} 1 & \cdots & 1 \end{bmatrix}^T\in R^n$$

$$W_{BW}=\begin{bmatrix} 0_n \\ \dfrac{-(1-\alpha)[k_{11}(I_0-i)+k_{10}]Dz(t)}{m_1} \\ 0_{n-1} \end{bmatrix}$$

### *3.2 The design of controller based on Lyapunov function*

The block diagram of the close-loop semi-active control system for a structure equipped with MRE base isolators is shown in Fig. 4. The civil structure is the plant and MRE base isolator is used as an actuator. Because the relative coordinate is selected to describe the motion, the disturbance $\ddot{x}_g$ the acceleration of ground impacts on both the MRE base isolator and the structure. The MRE base isolator changes the stiffness $k_1$ and damping coefficient $c_1$ between the

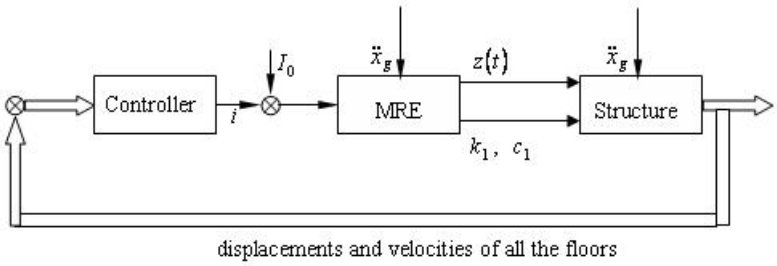


Fig. 4 Block diagram of the close-loop semi-active control system for a structure equipped with MRE

structure and ground by the applied current and at the same time the MRE generates auxiliary hysteretic force to the structure. The hysteretic force is related to the evolutionary variable $z(t)$. The applied current is $I_0$-$i$, where $I_0$ is the constant current supplied for MRE when there's no earthquakes. $i$ is the control current. The controller utilizes the displacement and velocity of each floor as the feedback and calculates the control current $i$ based on the Lyapunov's direct method which is detailed as followings.

Choose a positive-definite symmetric matrix P and Lyapunov function

$$V = x^T Px \tag{10}$$

The derivative of $V$ is expressed as

$$\begin{aligned}\dot{V} &= \dot{x}^T Px + x^T P\dot{x} \\ &= \left(Ax + b(x)i + W_{BW} + W_e\right)^T Px + x^T P\left(Ax + b(x)i + W_{BW} + W_e\right) \\ &= \left[x^T A^T + b^T(x)i + \left(W_{BW} + W_e\right)^T\right]Px + x^T P\left(Ax + b(x)i + W_{BW} + W_e\right) \\ &= x^T\left(A^T P + PA\right)x + \left[b^T(x)i + \left(W_{BW} + W_e\right)^T\right]Px + x^T P\left[b(x)i + W_{BW} + W_e\right]\end{aligned} \tag{11}$$

Note that $\left[b^T(x)i + \left(W_{BW} + W_e\right)^T\right]Px$ is a scalar, that is

$$\left[b^T(x)i + \left(W_{BW} + W_e\right)^T\right]Px = \left[\left[b^T(x)i + \left(W_{BW} + W_e\right)^T\right]Px\right]^T = x^T P\left(b(x)i + W_{BW} + W_e\right)$$

Therefore, Eq. (11) can be rewritten as

$$\dot{V} = x^T\left(A^T P + PA\right)x + 2x^T P\left(b(x)i + W_{BW} + W_e\right) \tag{12}$$

$$\dot{V} = -x^T Qx + 2x^T P\left(b(x)i + W_{BW} + W_e\right) \tag{13}$$

Where $A^TP+PA=-Q$

According to Rayleigh-Ritz theorem, Eq. (13) becomes

$$\dot{V} \le -\lambda_{\min}\|x\| + 2x^T P\left(b(x)i + W_{BW} + W_e\right) \tag{14}$$

where $\lambda_{\min}$ is the minimum of the eigenvalue of $Q$

To ensure $\dot{V} < 0$

Table 1 Boundedness of the hysteretic part of the Bouc-Wen model

| | Case | Ω | $\lvert z(t)\rvert$ bound | Class |
|---|---|---|---|---|
| $\theta>0$ | $\beta+\lambda>0$ and $\beta-\lambda\geq 0$ | $R$ | $\max(\lvert z(0)\rvert, z_0)$ | I |
| | $\beta-\lambda<0$ and $\beta\geq 0$ | $[-z_1, z_1]$ | $\max(\lvert z(0)\rvert, z_0)$ | II |
| $\theta<0$ | $\beta-\lambda>0$ and $\beta+\lambda\geq 0$ | $R$ | $\max(\lvert z(0)\rvert, z_1)$ | III |
| | $\beta+\lambda<0$ and $\beta\geq 0$ | $[-z_0, z_0]$ | $\max(\lvert z(0)\rvert, z_1)$ | IV |
| $\theta=0$ | $\beta+\lambda\geq 0$ and $\beta-\lambda\geq 0$ | $R$ | $\lvert z(0)\rvert$ | V |
| | All other cases | ∅ | | |

$$\begin{aligned} x^T P(b(x)i + W_{BW} + W_e) < 0 \\ x^T Pb(x)i < -x^T P(W_{BW} + W_e) \end{aligned} \tag{15}$$

According to Ismail *et al*. (2009), the $z(t)$ is uniformly bounded for any piecewise continuous signals $u_1$ and $\dot{u}_1$ (bounded or not) if parameters of Eq. (1) verify the inequalities in Table 1.

$z_0$ is defined as $z_0 = \sqrt[n]{\theta/(\beta+\lambda)}$ and $z_1$ is $z_1 = \sqrt[n]{\theta/(\lambda-\beta)}$. Ω denotes the set of initial conditions $z(0)$ for which the signal $z(t)$ is bounded for every piece wise continuous signal $\dot{x}$.

It was emphasized by Ismail *et al*. (2009) that only classes I and II behave in accordance with experimental observations of a base-isolation system, so the assumption for $z(t)$ is bounded is suitable for the MRE base isolator. There is a physical limitation of the supplied current for MRE, i.e.,

$$\lvert -(1-\alpha)[k_{11}(I_0 - i) + k_{10}]Dz(t)\rvert < (1-\alpha)(k_{11}I_{\max} + k_{10})D\max(\lvert z(t)\rvert)$$

where $I_{\max}$ is the maximum current applied to MRE. And accordingly $W_{BW}$ is bounded, $W_{BW}+W_e$ is bounded.

Define

$$\lVert W_{BW} + W_e\rVert < R_{dis} \tag{16}$$

Note that $x^{\mathrm{T}}P(W_{BW}+W_e)$ is a scalar

$$\begin{aligned} x^T P(W_{BW} + W_e) < \lVert x^T P(W_{BW} + W_e)\rVert \leq \lVert x^T P\rVert\lVert W_{BW} + W_e\rVert < \lVert Px\rVert R_{dis} \\ -\lVert Px\rVert R_{dis} < -x^T P(W_{BW} + W_e) \end{aligned} \tag{17}$$

Eq. (15) follows if $x^T Pb(x)i = -\lVert Px\rVert R_{dis}$ and so

$$i = -(x^T Pb(x))^{-1}\lVert Px\rVert R_{dis}$$

According to the physical limits of MRE, the applied current should not be negative or greater than the maximum current the coil can support. Therefore, analysis will be taken under such conditions.

(1) The applied current is $I_{\max}$

If the applied current is $I_{\max}$, that is to say the current is the maximum the MRE can endures, then the control current is $i=I_0-I_{\max}$, the matrix notations of Eq. (9) becomes

$$\dot{x} = Ax + b\left(I_0 - I_{\max}\right) + W_{BW} + W_e \tag{18}$$

Choose the same positive-definite symmetric matrix P and Lyapunov function as Eq. (10).

The derivative of $V$ is computed as follows

$$\begin{aligned}
\dot{V} &= \dot{x}^T Px + x^T P\dot{x} \\
&= \left(Ax + b(x)\left(I_0 - I_{\max}\right) + W_{BW} + W_e\right)^T Px + x^T P\left(Ax + b(x)\left(I_0 - I_{\max}\right) + W_{BW} + W_e\right) \\
&= \left[x^T A^T + \left(b(x)\left(I_0 - I_{\max}\right) + W_{BW} + W_e\right)^T\right]Px + x^T P\left(Ax + b(x)\left(I_0 - I_{\max}\right) + W_{BW} + W_e\right) \\
&= x^T\left(A^T P + PA\right)x + \left(b(x)\left(I_0 - I_{\max}\right) + W_{BW} + W_e\right)^T Px + x^T P\left(b(x)\left(I_0 - I_{\max}\right) + W_{BW} + W_e\right) \\
&= x^T\left(A^T P + PA\right) + 2x^T P\left(b(x)\left(I_0 - I_{\max}\right) + W_{BW} + W_e\right) \\
&= -\lambda_{\min}\|x\|^2 + 2x^T P\left(b(x)\left(I_0 - I_{\max}\right) + W_{BW} + W_e\right)
\end{aligned} \tag{19}$$

where $\lambda_{\min}$ is the minimum of the eigenvalue of $Q$ defined in Eq. (13).

If $\dot{V} < 0$, $x$ should meet

$$2x^T P\left(b(x)\left(I_0 - I_{\max}\right) + W_{BW} + W_e\right) < \lambda_{\min}\|x\|^2$$

From Eq. (16), it can be found that

$$\begin{gathered}
2x^T P\left(W_{BW} + W_e\right) < 2\|Px\|R_{dis} \\
2x^T P\left(b(x)\left(I_0 - I_{\max}\right)\right) \le 2\|P\|\|x\|\|b(x)\|\left|I_0 - I_{\max}\right| \\
2x^T P\left(b(x)\left(I_0 - I_{\max}\right) + W_{BW} + W_e\right) < 2\|P\|\|x\|R_{dis} + 2\|P\|\|x\|\|b(x)\|\left|I_0 - I_{\max}\right|
\end{gathered} \tag{20}$$

Take Eq. (19) into consideration, the following inequality is obtained if $\dot{V} < 0$

$$2\|P\|\|x\|\left(R_{dis} + \|b(x)\|\left|I_0 - I_{\max}\right|\right) < \lambda_{\min}\|x\|^2 \tag{21}$$

The following will show that $\|b(x)\|$ is bounded.

If the applied current is $I_{\max}$, Eq. (18) can be rewritten as

$$\dot{x} = A'x + Bu$$

where

$$A' = \begin{bmatrix} 0_n & I_n \\ -M^{-1}K_n' & -M^{-1}C_n' \end{bmatrix}$$

$$B = \begin{bmatrix} 0_n & 0_n \\ -1 & -1 \\ 0_{n-1} & -1_{n-1} \end{bmatrix}$$

$$1_{n-1} = \begin{bmatrix} 1 & \cdots & 1 \end{bmatrix}^T \in R^{n-1}$$

$$u=\begin{bmatrix}(1-\alpha)(k_{11}I_{\max}+k_{10})Dz(t)\\ \ddot{x}_g\end{bmatrix}$$

$$M=\begin{bmatrix}m_1 & & & & & & \\ & m_2 & & & & & \\ & & \ddots & & & & \\ & & & m_j & & & \\ & & & & \ddots & & \\ & & & & & m_{n-1} & \\ & & & & & & m_n\end{bmatrix}$$

$$K_n'=\begin{bmatrix}\alpha(k_{11}I_{\max}+k_{10})+k_2 & -k_2 & \cdots & 0 & \cdots & 0 & 0\\ -k_2 & k_2+k_3 & \cdots & 0 & \cdots & 0 & 0\\ \vdots & \vdots & \ddots & \vdots & \cdots & \vdots & \vdots\\ 0 & 0 & \cdots & k_j+k_{j+1} & \cdots & 0 & 0\\ \vdots & \vdots & \cdots & \vdots & \ddots & \vdots & \vdots\\ 0 & 0 & \cdots & 0 & \cdots & k_{n-1}+k_n & -k_n\\ 0 & 0 & \cdots & 0 & \cdots & -k_n & k_n\end{bmatrix}\in R^{n\times n}$$

$$C_n'=\begin{bmatrix}(c_{11}I_{\max}+c_{10})+c_2 & -c_2 & \cdots & 0 & \cdots & 0 & 0\\ -c_2 & c_2+c_3 & \cdots & 0 & \cdots & 0 & 0\\ \vdots & \vdots & \ddots & \vdots & \cdots & \vdots & \vdots\\ 0 & 0 & \cdots & c_j+c_{j+1} & \cdots & 0 & 0\\ \vdots & \vdots & \cdots & \vdots & \ddots & \vdots & \vdots\\ 0 & 0 & \cdots & 0 & \cdots & c_{n-1}+c_n & -c_n\\ 0 & 0 & \cdots & 0 & \cdots & -c_n & c_n\end{bmatrix}\in R^{n\times n}$$

As Soong (1990) pointed out, for civil structures the *i*th eigenvalues of the matrix *A'*, $p_i$($i$=1,2,…,$n$), are given by the following complex conjugage pairs

$$p_i=-\xi_i\omega_{ji}\pm j\omega_i\sqrt{1-\xi_i^2}$$

Because the real part of eigenvalue of *A'* is negative, the system is Bounded input-bounded output (BIBO). That is to say $x$ is bounded when $u=\begin{bmatrix}(1-\alpha)(k_{11}I_{\max}+k_{10})Dz(t)\\ \ddot{x}_g\end{bmatrix}$ is bounded.

Accordingly $b(x)=\begin{bmatrix}0_n\\ \dfrac{c_{11}\dot{u}_1+\alpha k_{11}u_1}{m_1}\\ 0_{n-1}\end{bmatrix}$ is bounded.

If $\|b(x)\|$ is bounded, i.e., $\|b(x)\| < R_b$, Eq. (20) becomes

$$2\|P\|\|x\|\left(R_{dis} + \|b(x)\|(I_0 - I_{\max})\right) < 2\|P\|\|x\|\left(R_{dis} + R_b(I_0 - I_{\max})\right)$$

Combine with Eq. (21), the following inequality is obtained

$$2\|P\|\|x\|\left(R_{dis} + R_b(I_0 - I_{\max})\right) < \lambda_{\min}\|x\|^2$$

$$\|x\| > \frac{2\|P\|\left(R_{dis} + R_b(I_0 - I_{\max})\right)}{\lambda_{\min}}$$

If the applied current is $I_{\max}$ and the norm of $x$ is large enough, the system will converge to $\frac{2\|P\|\left(R_{dis} + R_b(I_0 - I_{\max})\right)}{\lambda_{\min}}$

(2) The applied current is zero

If the applied current is zero, $i=I_0-0=I_0$, the matrix notations of Eq. (9) become

$$\dot{x} = Ax + bI_0 + W_{BW} + W_e \tag{22}$$

Choose the same positive-definite symmetric matrix P and Lyapunov function as Eq. (10). The derivative of $V$ is computed as follows

$$\begin{aligned}
\dot{V} &= \dot{x}^T Px + x^T P\dot{x} \\
&= \left(Ax + b(x)I_0 + W_{BW} + W_e\right)^T Px + x^T P\left(Ax + b(x)I_0 + W_{BW} + W_e\right) \\
&= \left[x^T A^T + \left(b(x)I_0 + W_{BW} + W_e\right)^T\right]Px + x^T P\left(Ax + b(x)I_0 + W_{BW} + W_e\right) \\
&= x^T\left(A^T P + PA\right)x + \left(b(x)I_0 + W_{BW} + W_e\right)^T Px + x^T P\left(b(x)I_0 + W_{BW} + W_e\right) \\
&= x^T\left(A^T P + PA\right) + 2x^T P\left(b(x)I_0 + W_{BW} + W_e\right) \\
&= -\lambda_{\min}\|x\|^2 + 2x^T P\left(b(x)I_0 + W_{BW} + W_e\right)
\end{aligned} \tag{23}$$

Where $\lambda_{\min}$ is the minimum of the eigenvalue of $Q$ defined in Eq. (13).

If $\dot{V} < 0$, $x$ should meet

$$2x^T P\left(b(x)I_0 + W_{BW} + W_e\right) < \lambda_{\min}\|x\|^2$$

From Eq. (16), it can be found that

$$\begin{aligned}
2x^T P\left(W_{BW} + W_e\right) &< 2\|Px\|R_{dis} \\
2x^T P\left(b(x)I_0\right) &< 2\|P\|\|x\|\|b(x)\|I_0| \\
2x^T P\left(b(x)I_0 + W_{BW} + W_e\right) &< 2\|P\|\|x\|R_{dis} + 2\|P\|\|x\|\|b(x)\|I_0|
\end{aligned} \tag{24}$$

Take Eq. (23) into consideration, the following inequality is obtained if $\dot{V} < 0$

$$2\|P\|\|x\|\left(R_{dis} + \|b(x)\|I_0|\right) < \lambda_{\min}\|x\|^2 \tag{25}$$

As the previous section shows that $\|b(x)\|$ is bounded, that is $\|b(x)\| < R_b$, Eq. (24) becomes

$$2\|P\|\|x\|\left(R_{dis}+\|b(x)\|I_0\right)<2\|P\|\|x\|\left(R_{dis}+R_bI_0\right)$$

Combine with Eq. (24), the following inequality is obtained

$$2\|P\|\|x\|\left(R_{dis}+R_bI_0\right)<\lambda_{\min}\|x\|^2$$

$$\|x\|>\frac{2\|P\|\left(R_{dis}+R_bI_0\right)}{\lambda_{\min}}$$

If the supply current is zero and the norm of $x$ is large enough, the system will converge to $\frac{2\|P\|\left(R_{dis}+R_bI_0\right)}{\lambda_{\min}}$

## 4. Case studies

A six-storey benchmark building (Kelly *et al*. 1987, Ramallo *et al*. 2002, Li *et al*. 2006) is used to examine the effectiveness of the proposed controller. Table 2 lists all the parameters of structure. Two far-field and two near-field historical records are selected to excite the benchmark model: (1) El Centro, N-S component recorded on May 18, 1940. (2) Hachinohe, N-S component recorded on May 16, 1968. (3) Northridge, N-S component recorded on January 17, 1994. (4) Kobe, N-S component recorded on January 17, 1995. All the excitations are applied with the full intensity for the evaluation of the performance of the proposed system.

To demonstrate the superiority of the adaptive base isolation system, its performance is compared with two passive base isolation systems, i.e., Case 1: an optimal passive base isolation system and Case 2: a passive base isolation system with equivalent base shear of the adaptive base isolation system. The passive base isolation system consists of base isolator and superstructure. The isolator lies between the superstructure and the ground and decouples the structure from the horizontal components of the ground motion by interposing structural elements with low horizontal stiffness. The fundamental frequency of the passive base system is much lower than both fixed-base frequency and the predominant frequencies of the ground motion. The stiffness and damping coefficients 232 KN/m, 3.74 KN s/m of the optimal passive system proposed by Ramallo (Ramallo *et al*. 2002) are used in Case 1.

One of the challenges in the design of base isolation system is how to reduce the drift of base isolation while the rigid motion of superstructure is maintained. The passive base isolation system often possesses large drift in the base floor due to the mechanism of the base isolation system, e.g., low lateral stiffness of the base isolation system to create lower fundamental frequency of the entire system. However, large drift in the base isolators also creates instability of the base isolation

Table 2 Structural Model Parameters of the six-storey benchmark building model

| | Floor 1 (isolation floor) | Floor 2 | Floor 3 | Floor 4 | Floor 5 | Floor 6 |
|---|---|---|---|---|---|---|
| mass(Kg) | 6800 | 5897 | 5897 | 5897 | 5897 | 5897 |
| Stiffness coefficients(KN/m) | 232 | 33732 | 29093 | 28621 | 24954 | 19059 |
| Damping coefficients(KN s/m) | 3.74 | 68 | 58 | 57 | 50 | 38 |

system. Therefore, in Case 2 the stiffness coefficient of passive base isolation system is modified to maintain similar drift as the adaptive base isolation system. The performances of two systems are then compared using the criteria described in the following session.

$$J_1 = \max\left\{\frac{\max\limits_{t,i}\left|d_i(t)\right|}{d_i^{\max}}\right\}$$

$$J_2 = \max\left\{\frac{\max\limits_{t,i}\left|\ddot{x}_{ai}(t)\right|}{\ddot{x}_a^{\max}}\right\}$$

$$J_3 = \max\left\{\frac{\max\limits_{t}\left|\sum\limits_{i=1}^{6} m_i\ddot{x}_{ai}(t)\right|}{F_b^{\max}}\right\}$$

$$J_4 = \max\left\{\frac{\max\limits_{i}\left\|d_i(t)\right\|}{\left\|d_i^{\max}\right\|}\right\}$$

$$J_5 = \max\left\{\frac{\max\limits_{i}\left\|\ddot{x}_{ai}(t)\right\|}{\left\|\ddot{x}_a^{\max}\right\|}\right\}$$

$$J_6 = \max\left\{\frac{\left\|\sum\limits_{i=1}^{6} m_i\ddot{x}_{ai}(t)\right\|}{\left\|F_b^{\max}\right\|}\right\}$$

$J_1$ to $J_6$ are categorised as the criteria based on the response of the building, among which $J_1$ to $J_3$ are related to the peak building response while $J_4$ to $J_6$ represent the normed structural responses. In other words, $J_2$ and $J_3$ indicate the peak floor acceleration ratio and peak base shear ratio between the semi-active control and passive control structure. Meanwhile, $J_5$ and $J_6$ are the normalised floor acceleration and base shear ratio of the semi-active control and passive control base isolation system. The meanings of each symbol in the equation are listed as following.

$d_i(t)$: inter-storey drift of the i-th floor with semi-active control

$d_i^{\max}$: the maximum inter-storey drift of the i-th floor with passive control

$\ddot{x}_{ai}(t)$: acceleration of the i-th floor with semi-active control

$\ddot{x}_a^{\max}$ : the maximum acceleration of the i-th floor with passive control

$F_b^{\max}$: maximum base shear of the passive controlled structure for each respective earthquake

$m_i$: seismic mass of the i-th floor above ground floor

In the normed response evaluative indices, the norm, $\|\bullet\|$, is computed using the following equation

$$\|\bullet\| = \sqrt{\frac{1}{t_f}\int_0^{t_f}[\bullet]^2\,dt}$$

where $t_f$ is a time period large enough to allow the response of the structure to attenuate.

### 4.1 Performance of semi-active control vs optimal passive base isolation systems

Due to the page limit, only the time histories of two systems under El Centro earthquake shown in Fig. 5 are presented here. Time histories of the relative displacement and acceleration responses of the benchmark building for semi-active control and passive control with optimal coefficients are shown in Figs. 6-7. It is clear from the time histories that the semi-active strategy capable of varying the stiffness of base isolation system provides moderate reduction of the maximum displacement and acceleration. For example, Fig. 6 indicates reductions in building peak displacement, i.e., 53.92%, 53.77%, 53.65%, 53.57%, 53.51% and 53.47%, for the first to the sixth floor, respectively, when compared with the passive control. Fig. 6 also gives the response when the applied current MRE is zero and maximum. It can be seen that the system is not stable when the applied current is zero. The reason is that the stiffness of MRE is too small to maintain real part of the eigenvalue of the state matrix negative when the applied current is zero. The frequency of the oscillatory motion of the structure is highest when the MRE is applied with the maximum current because the fundamental natural frequency is proportional to the stiffness. All the responses of acceleration of different floors are reduced with the help of semi-active control, which can be observed visually from Fig. 7. The applied current of MRE, i.e., $I_0$-$i$ is shown in Fig. 8. Similar significant reductions under the other three earthquakes are also obtained. The reduction in the peak base displacement of the base-isolated building is one of the most important criteria during strong earthquakes.

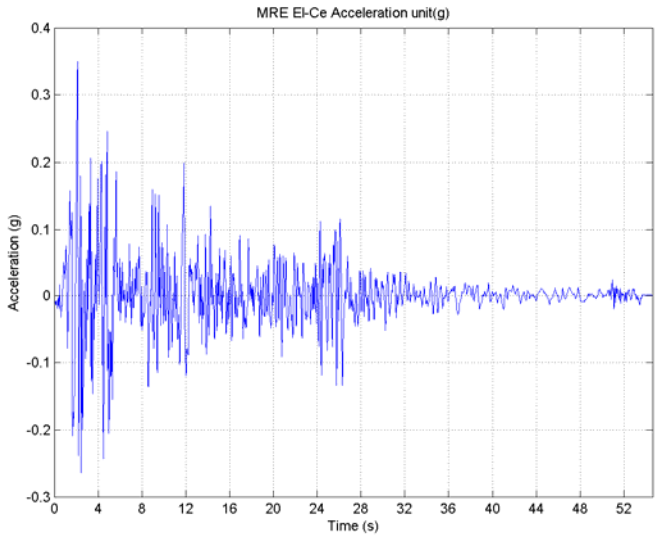


Fig. 5 Ground Acceleration of El Centro

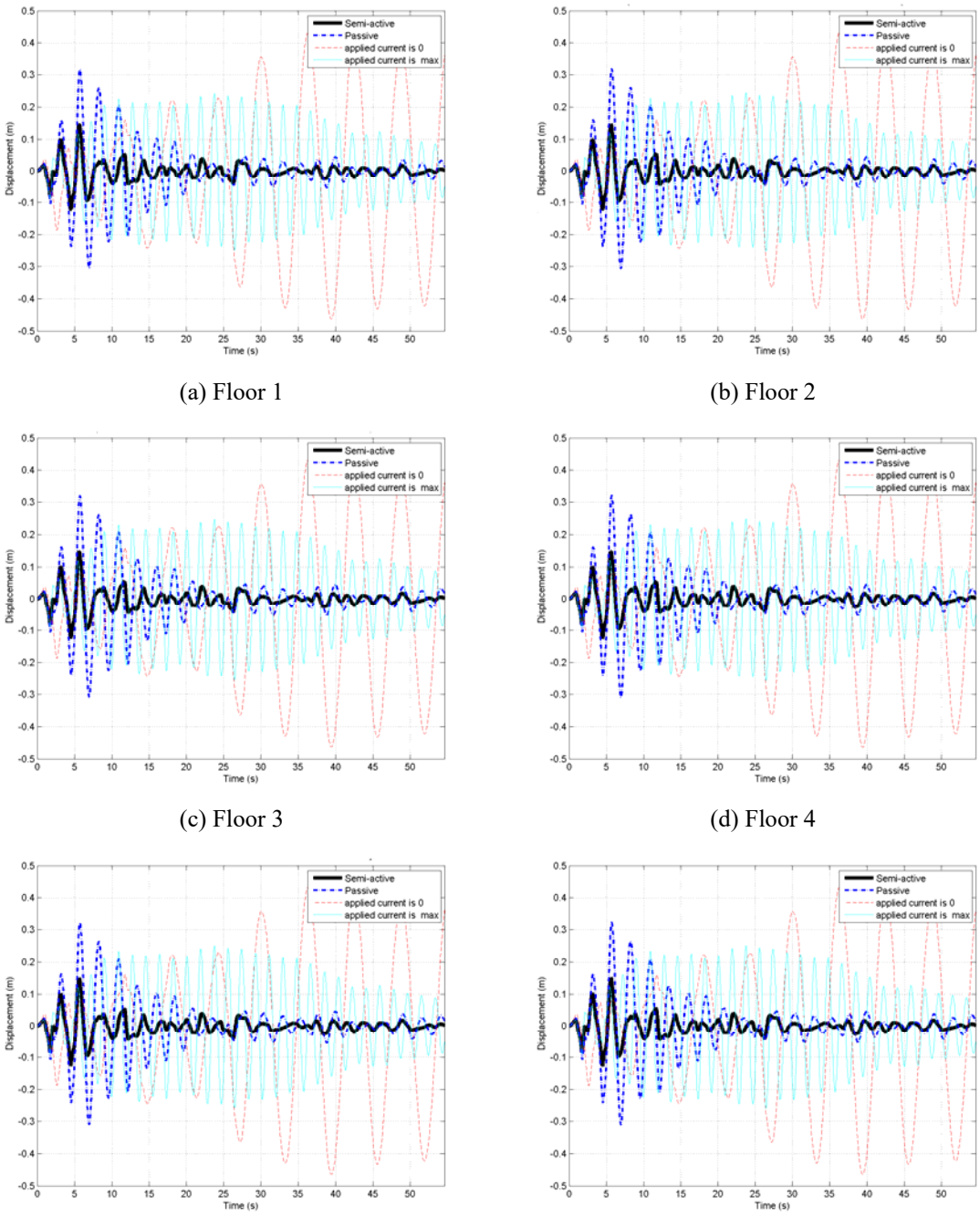


(a) Floor 1 (b) Floor 2

(c) Floor 3 (d) Floor 4

(e) Floor 5 (f) Floor 6

Fig. 6 The time histories of relative displacements of El Centro for adaptive base isolation system, optimal passive base isolation system, the applied current of MRE is zero and the applied current of MRE is the maximum

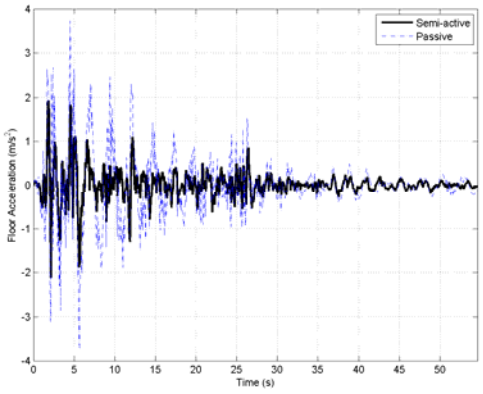


(a) Floor 1

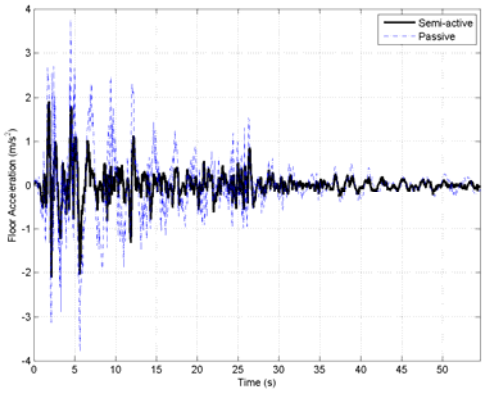


(b) Floor 2

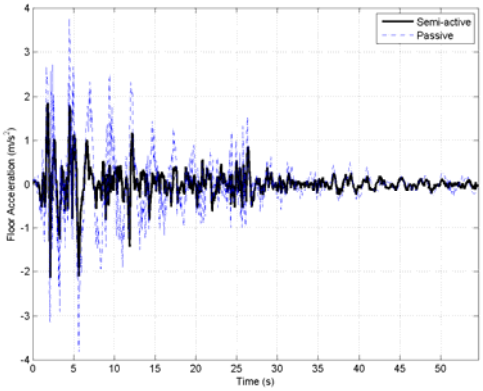


(c) Floor 3

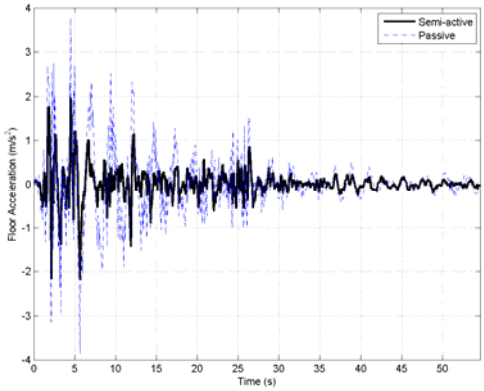


(d) Floor 4

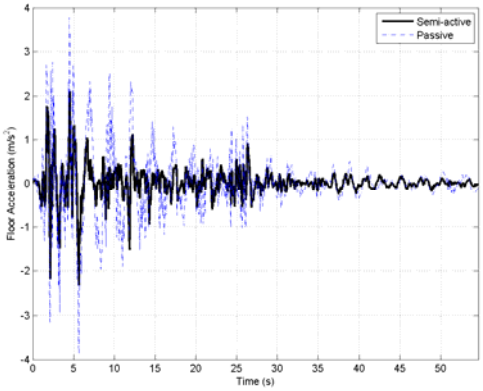


(e) Floor 5

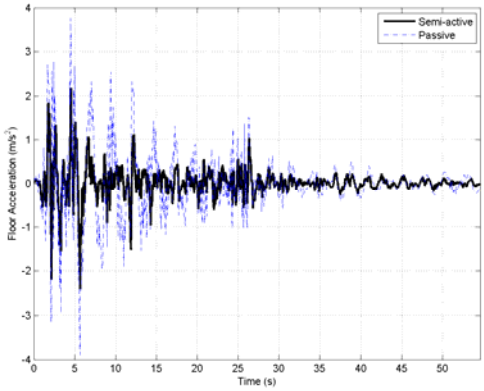


(f) Floor 6

Fig. 7 The time histories of acceleration of El Centro for adaptive base isolation system and optimal passive base isolation system

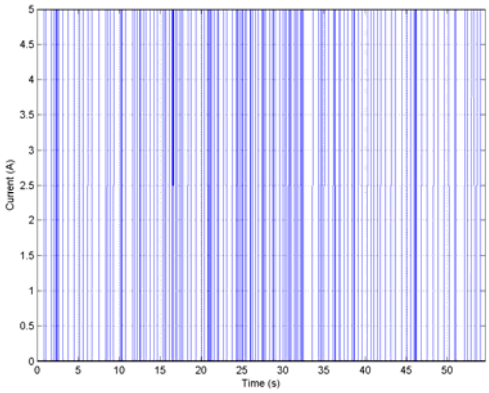


Fig. 8 The applied current for El Centro Earthquake

Table 3 Comparison (in ratio) between the adaptive base isolation system and the optimal passive base isolation against all evaluation criteria

| | J1 | J2 | J3 | J4 | J5 | J6 |
|---|---|---|---|---|---|---|
| El-centro | 0.461 | 0.619 | 0.558 | 0.353 | 0.497 | 0.484 |
| Hachinohe | 0.240 | 0.465 | 0.407 | 0.224 | 0.282 | 0.270 |
| Northridge | .0.440 | 0.664 | 0.588 | 0.245 | 0.339 | 0.330 |
| Kobe | 0.627 | 0.694 | 0.660 | 0.653 | 0.690 | 0.684 |

The evaluation criteria (performance indices) defined above are listed in Table 3. It is obvious from Table 3 that in terms of the J1, J2, J3, under all four earthquakes, near-field or far-field, the Lyapunov-based controlled system has significantly reduced the maximum structural response of floor displacement, acceleration and base shear. The benefit of Lyapunov-based strategy is the reduction in base displacements without an increase in drift J1, which is desirable for practical applications. Because normed value is a statistical measure of the magnitude of response over the statistical range, the indices of J4, J5 and J6 are able to better evaluate the responses along the entire time history. The normed indices of Lyapunov-based system are smaller than that of passive system, which indicates that the Lyapunov-based controller holds advantage over the passive one during the whole period of the earthquakes.

Additionally, the peak accelerations of each floor are calculated and shown in Fig. 9. Compared with the passive system, the response of the peak acceleration of each floor in the Lyapunov-based system is significantly reduced. The peak acceleration of the different floor of the passive system increases with the floor number. The similar phenomenon can't be observed in the Lyapunov-based system. For example, the minimum response of peak acceleration occurs on the fourth floor under the Hachinohe earthquake.

The inter-storey drift which shows the deformation between the adjacent floors are calculated and listed in Table 4. Table 4 contains the inter-storey drift from floor 1 to floor 6 and it can be clearly observed that the peak inter-storey drifts of the Lyapunov-based control and passive control occur at the isolation floor i.e. floor 1 under all earthquakes, which implies the base isolation are effective. The Lyapunov-based controller achieves considerable reduction of the peak inter-storey

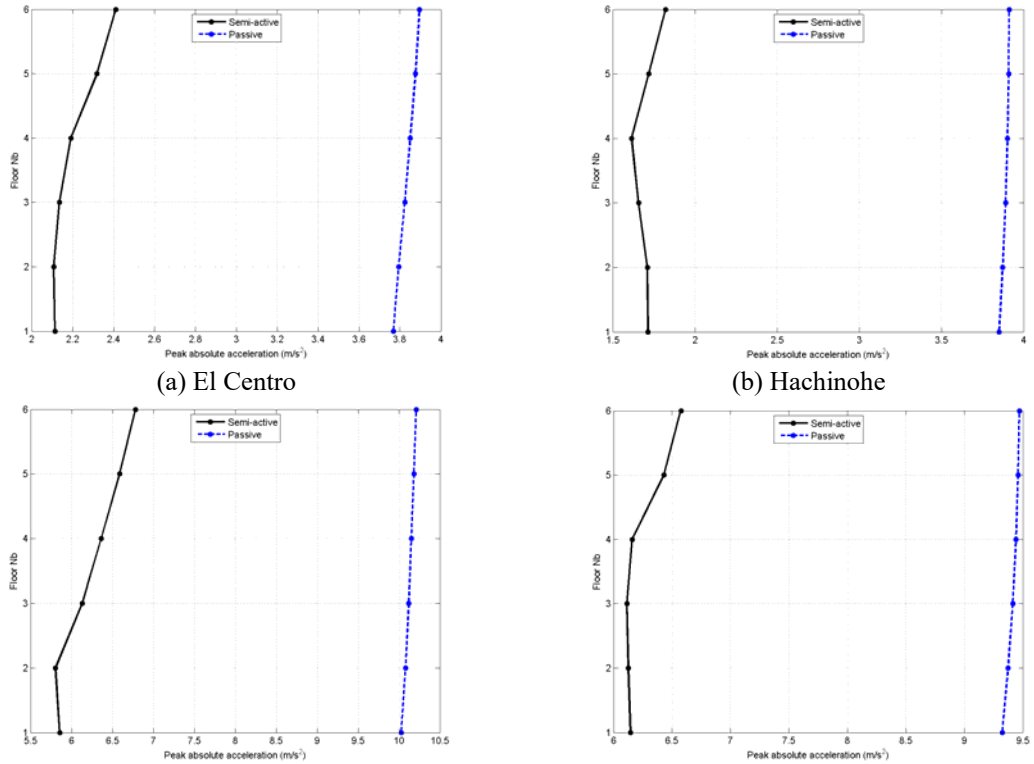


(a) El Centro (b) Hachinohe

(c) Northridge (d) Kobe

Fig. 9 The peak acceleration of different floor

Table 4 Inter-storey drift from floor 1 to floor 6 (Unit: mm)

| | Floor 1 (isolation floor) | | Floor 2 | | Floor 3 | | Floor 4 | | Floor 5 | | Floor 6 | |
|---|---|---|---|---|---|---|---|---|---|---|---|---|
| | Passive | Semi-Active | Passive | Semi-Active | Passive | Semi-Active | Passive | Semi-Active | Passive | Semi-Active | Passive | Semi-Active |
| El-centro | 314.867 | 145.982 | 1.766 | 1.324 | 1.646 | 1.298 | 1.260 | 1.076 | 0.967 | 0.856 | 0.635 | 0.754 |
| Hachinohe | 562.092 | 134.419 | 3.152 | 1.234 | 2.931 | 1.355 | 2.240 | 1.360 | 1.716 | 1.340 | 1.125 | 0.984 |
| Northridge | 973.569 | 426.828 | 5.465 | 3.977 | 5.082 | 3.941 | 3.882 | 3.153 | 2.972 | 2.659 | 1.949 | 2.409 |
| Kobe | 380.2100 | 238.569 | 2.409 | 2.1500 | 2.562 | 2.010 | 2.105 | 1.542 | 1.757 | 1.186 | 1.215 | 0.780 |

drift compared with passive control. This is a valuable benefit since the excessive deformation of the base isolator may cause instability or even failure of the system.

### *4.2 Performances of semi-active and passive base isolation systems under same base drift*

In order to compare the inter-storey drift above floor 1 more objectively, the maximum base drifts of semi-active and passive system are set to be similar value in this case by modifying the stiffness matrix of the passive system. Fig. 10 and Fig. 11 display the time histories of relative

displacement and relative acceleration under El Centro. The reduction of relative displacement and acceleration is achieved by the Lyapunov-based system during the entire earthquake duration. The frequency of the response of Case 2 is higher than that of Case 1 because the stiffness and damping coefficients in Case 2 are not the optimal values as in Case 1. The rule of the design of the optimal passive base isolator is to balance the base displacement and the acceleration. If the stiffness is larger than the optimal value, the nature frequency becomes higher.

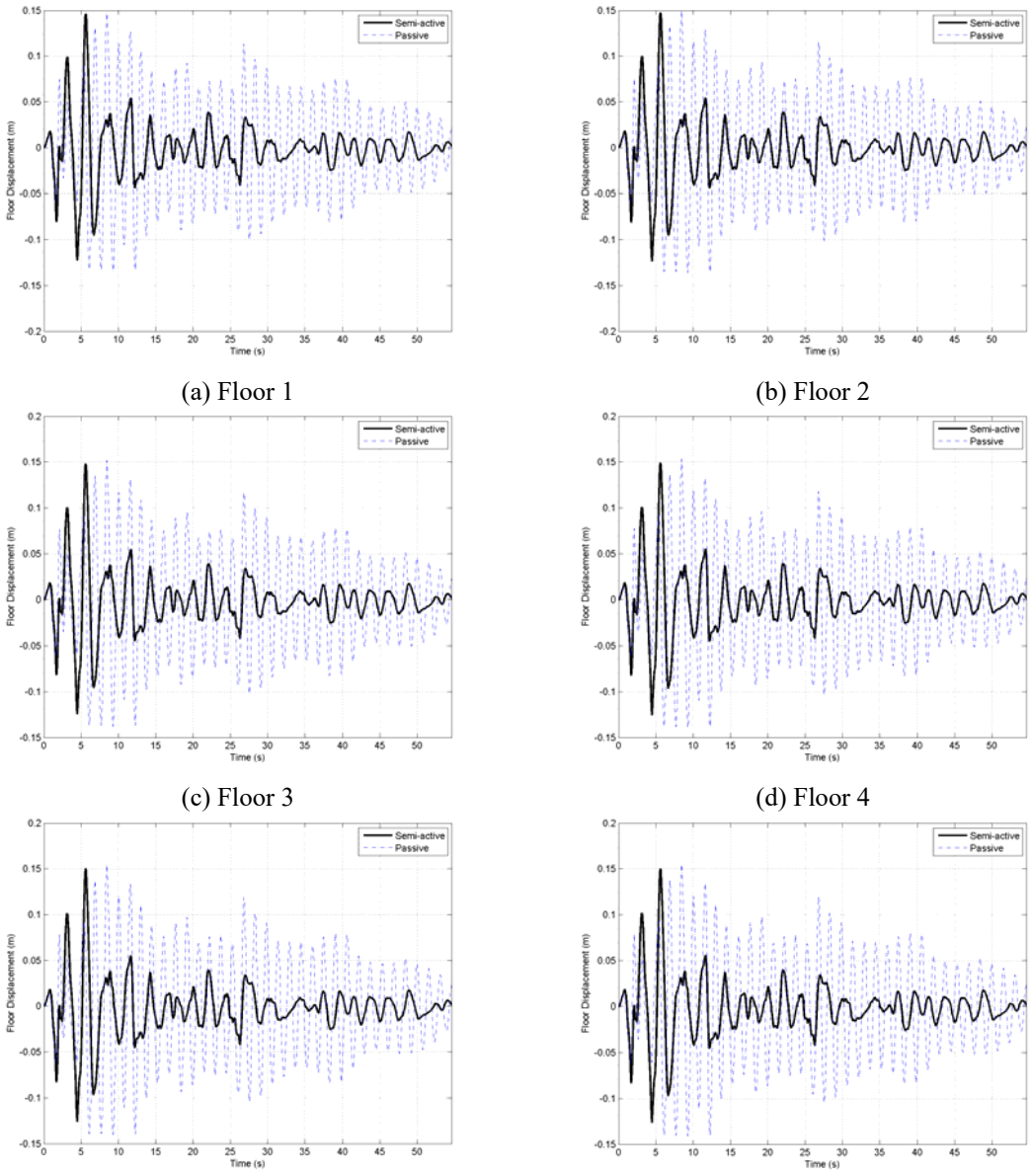


(a) Floor 1 (b) Floor 2

(c) Floor 3 (d) Floor 4

(e) Floor 5 (f) Floor 6

Fig. 10 The time histories of relative displacements of El Centro when the base drifts of two system are the same

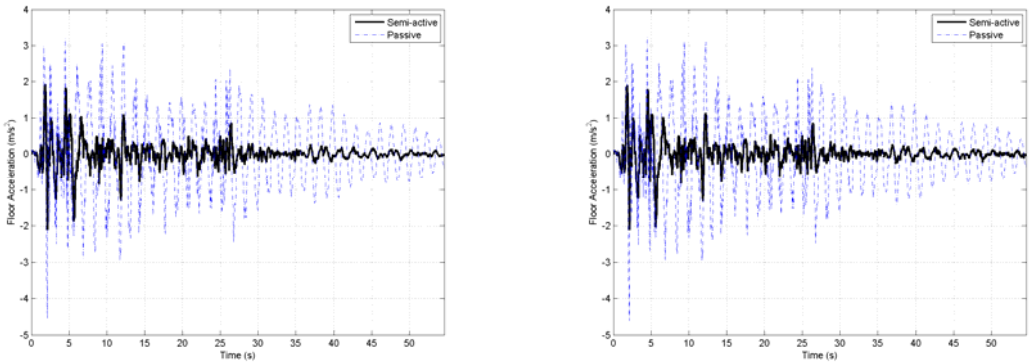


(a) Floor 1 (b) Floor 2

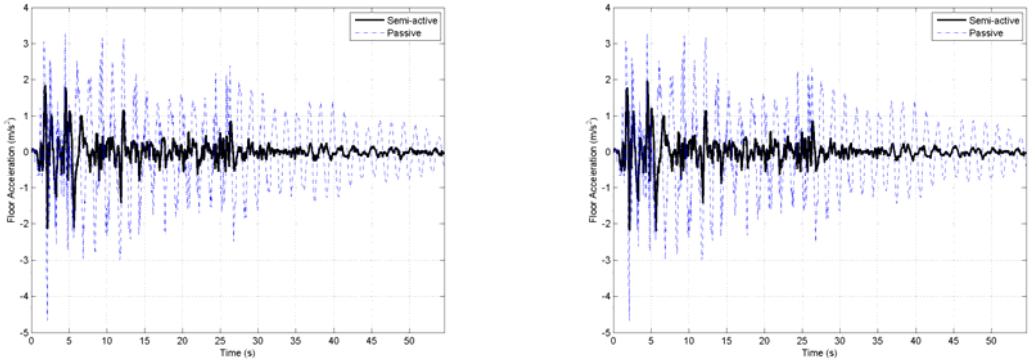


(c) Floor 3 (d) Floor 4

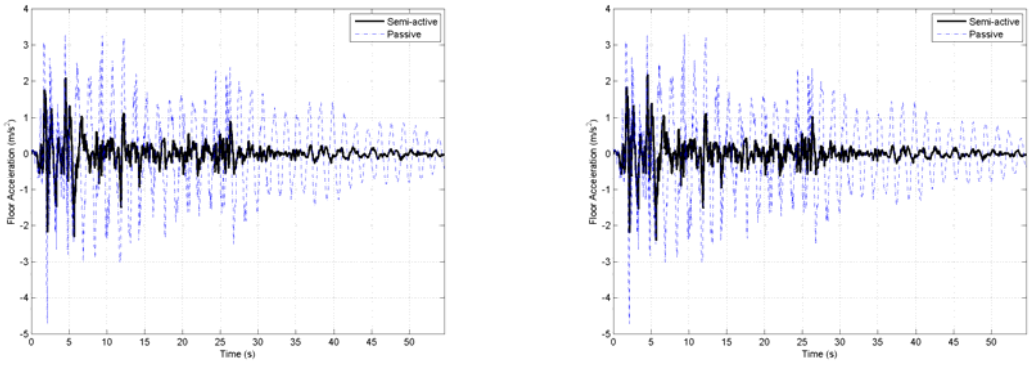


(e) Floor 5 (f) Floor 6

Fig. 11 The time histories of relative acceleration of El Centro when the base drifts of two systems are the same

Table 5 gives the detailed inter-storey drift from floor 1 to floor 6. The Lyapunov-based semi-active control achieves less inter-storey drift than that of passive control, which indicates the body motion of the superstructure on the MRE isolator is more like rigid body motion than that of

Table 5 Inter-storey drift from floor 1 to floor 6 when the base drifts of two systems are the same (Unit: mm)

| | Floor 1 (isolation floor) | | Floor 2 | | Floor 3 | | Floor 4 | | Floor 5 | | Floor 6 | |
|---|---|---|---|---|---|---|---|---|---|---|---|---|
| | Passive | Semi-Active | Passive | Semi-Active | Passive | Semi-Active | Passive | Semi-Active | Passive | Semi-Active | Passive | Semi-Active |
| El-centro | 147.641 | 147.641 | 2.221 | 1.324 | 2.072 | 1.298 | 1.586 | 1.076 | 1.217 | 0.856 | 0.799 | 0.754 |
| Hachinohe | 133.869 | 133.869 | 3.258 | 1.234 | 3.051 | 1.355 | 2.344 | 1.361 | 1.804 | 1.340 | 1.187 | 0.984 |
| Northridge | 427.308 | 427.308 | 9.267 | 3.977 | 8.676 | 3.941 | 6.666 | 3.153 | 5.130 | 2.659 | 3.375 | 2.409 |
| Kobe | 237.754 | 237.754 | 25.585 | 2.409 | 24.549 | 2.562 | 19.238 | 2.105 | 15.038 | 1.757 | 10.005 | 1.215 |

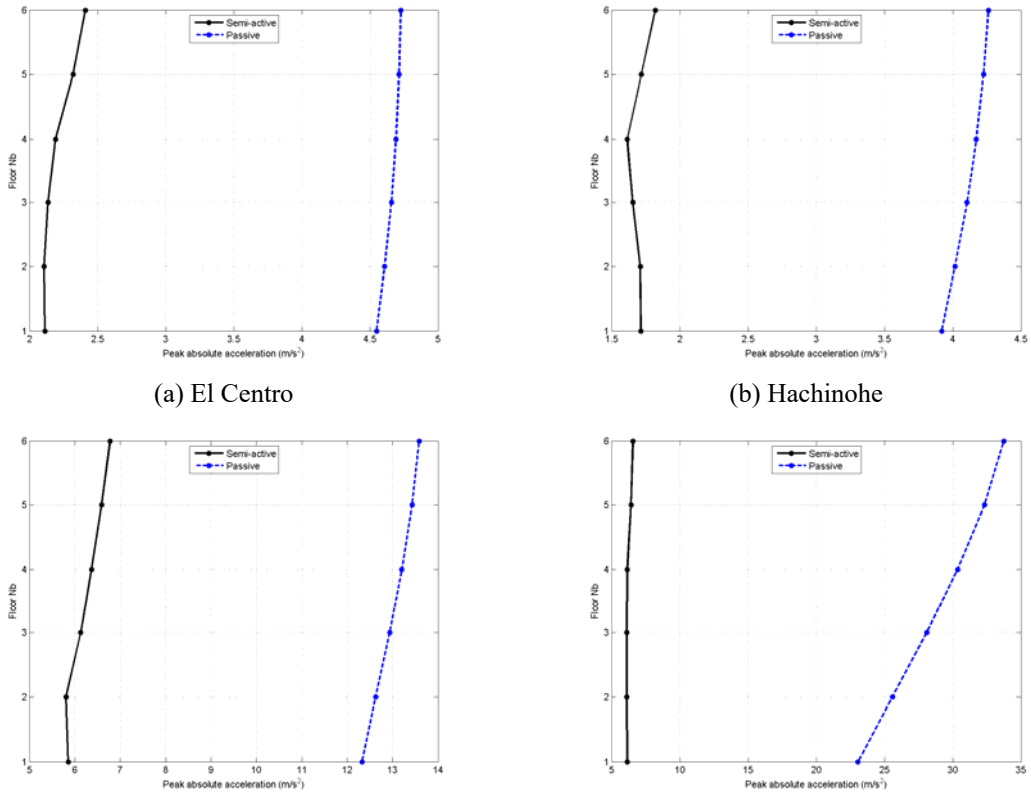


(a) El Centro (b) Hachinohe

(c) Northridge (d) Kobe

Fig. 12 The peak acceleration from when the base drift s of two systems are the same

passive isolator. Fig. 12 shows the response of peak acceleration from floor 1 to floor 6. As shown in all variations, the Lyapunov-based semi-active control system achieves considerable reduction of peak acceleration of each floor.

The evaluation criteria are calculated again in Case 2 and the results are shown in Table 6. $J_1$ is 1 because the base drift are the same in Case 2. All the values in Table 6 are smaller than one except $J_1$, which demonstrates that Lyapunov-based system shows a better performance to the passive system when the base drifts are the same.

Table 6 Comparison (in ratio) between the adaptive base isolation system and the optimal passive base isolation against all evaluation criteria under the constraint maximum isolator deformation

| | J1 | J2 | J3 | J4 | J5 | J6 |
|---|---|---|---|---|---|---|
| El-centro | 1 | 0.510 | 0.460 | 0.491 | 0.312 | 0.309 |
| Hachinohe | 1 | 0.427 | 0.385 | 0.601 | 0.314 | 0.309 |
| Northridge | 1 | 0.500 | 0.458 | 0.632 | 0.255 | 0.254 |
| Kobe | 1 | 0.195 | 0.216 | 0.626 | 0.128 | 0.144 |

## 5. Conclusions

This paper presented an investigation on utilisation a MRE base isolator in base isolation systems to produce adaptive base isolation system. With controllable lateral stiffness, the adaptive base isolation system will be capable of autonomously altering its system configuration by a feedback controller. In the paper, a Lyapunov-based controller was proposed and designed to adaptively drive the current applied to MRE base isolators and therefore control the lateral stiffness of the base isolators in real time. A numerical evaluation of the proposed adaptive base isolation system was carried out using a widely recognised benchmark base-isolated structure and examining all evaluation criteria. The results have shown that the performance of the adaptive base isolation system, implemented with the proposed control strategy, surpasses the optimal passive base isolation with or without the constraint on base drift. In conclusion, the MRE based adaptive isolation system can be a potential solution in overcoming shortcoming of popular passive base isolations to protect the civil structures under seismic events.

## Acknowledgements

This work was supported by Australian Research Council through Discovery Project (Grant No. DP150102636) as well as Blue Sky Research Fund from Faculty of Engineering and IT, University of Technology Sydney (UTS).

## References

Fabio, C., Jose, R. and Umut, Y. (2012), "Active and semi-active control of structures - theory and applications: A review of recent advances", *J. Intel. Mat. Syst. Struct.*, **23**(11), 1181-1195.

Faycal, I. (2007), *Systems with hysteresis analysis, identification and control using the Bouc-Wen model*, John Wiley & Sons Ltd, Chichester, England.

Fisco, N.R. and Adeli, H. (2011), "Smart structures: Part I-Active and semi-active control", *Sci. Iran.*, **18**(3), 275-284.

Gu, X., Li, J., Li, Y. and Askari, M. (2015), "Frequency control of smart base isolation system employing a novel adaptive magneto-rheological elastomer base isolator", *J. Intel. Mat. Syst. Struct.*, **27**(7), 849-858.

Hosseini, M. and Farsangi, E.N. (2012), "Telescopic columns as a new base isolation system for vibration control of high-rise buildings", *Earthq. Struct.*, **3**(6), 853-867.

Housner, G.W., Bergman, L.A., Caughey, T.K., Chassiakos A.G., Claus R.O., Masri S.F., Skelton R.E., Soong T.T., Spencer B.F. and Yao J.T.P. (1997), "Structural control: past, present, and future", *J. Eng.*

*Mech*., ASCE, **123**(9), 897-971.
Ismail, M., Ikhouane, F. and Rodellar, J. (2009), "The Hysteresis Bouc-Wen Model, a Survey", *Arch. Comput. Method E.*, **16**(2), 161-188.
Kelly, J.M., Leitmann, G. and Soldatos, A.G. (1987), "Robust control of base-isolated structures under earthquake excitation", *J. Optimiz, Theory App.*, **53**(2), 159-180.
Li, H. and Ou, J. (2006), "A design approach for semi-active and smart base-isolated buildings", *Struct. Control Hlth.*, **13**, 660-681
Li, Y. and Li, J. (2015a), "Finite element design and analysis of adaptive base isolator utilizing laminated multiple magnetorheological elastomer layers", *J. Intel. Mat. Syst. Str.*, **26**(14), 1861-1870.
Li, Y. and Li, J. (2015b), "A highly adjustable base isolator utilizing magnetorheological elastomer: experimental testing and modeling", *J. Vib. Acoust.*, **137**(1), 11009
Li, Y., Li, J., Li, W. and Samali, B. (2013a), "Development and characterization of a magnetorheological elastomer based adaptive seismic isolator", *Smart Mater. Struct.,* **22**, 035005.
Li, Y., Li, J., Tian, T. and Li, W. (2013b), "A highly adjustable magnetorheological elastomer base isolator for applications on real-time adaptive control", *Smart Mater. Struct.*, **22**, 095020.
Liu, J, Xia, K and Zhu, C. (2009), "The state-of-the-art review of structural control strategy", *International Conference on E-Learning, E-Business, Enterprise Information Systems, and E-Government*, HongKong, HongKong, December.
Murase, M., Tsuji, M. and Takewaki, I. (2013), "Smart passive control of buildings with higher redundancy and robustness using base-isolation and inter-connection", *Earthq. Struct.*, **4**(6), 649-670.
Patil, S.J., Reddy, G.R., Shivshankar, R., Rabu, R., Jayalekshmi, B.R. and Kumar, B. (2016), "Seismic base isolation for structures using river sand", *Earthq. Struct.*, **10**(4),829-847.
Ramallo, J.C., Johnson, E.A. and Spencer Jr, B.F. (2002), "'Smart' base isolation systems", *J. Eng. Mech*., ASCE, **128**(10), 1088-1099.
Soong, T.T. (1990), *Active structural control: theory and practice*, John Wiley & Sons Ltd, New York, USA.
Spencer Jr, B.F. and Nagarajaiah, S. (2003), "State of the art of structural control", *J. Struct. Eng*., ASCE, **129**(7), 845-856.
Sues, R., Mau, S., and Wen, Y. (1988), "Systems identification of degrading hysteretic restoring forces", *J. Eng. Mech*., ASCE, **114**(5), 833-846.
Tarek, E.S., George, N., Jan-Erik, J. and Hans, H. (2015), "A state-of-the-art review of structural control systems", *J. Vib. Control*, **21**(5), 919-937.
Yang, J., Du, H., Li, W., Li, Y. and Li, J. (2013), "Experimental study and modeling of a novel magnetorheological elastomer isolator", *Smart Mater. Struct.*, **22**(11), 117001.
Yu, Y., Li, Y. and Li, J. (2014), "A New Hysteretic Model for Magnetorheological Elastomer Base Isolator and Parameter Identification Based on Modified Artificial Fish Swarm Algorithm", *The 31st International Symposium on Automation and Robotics in Construction and Mining*, Sydney, July.
Yu Y., Li Y. and Li J. (2015b), "Parameter identification and sensitivity analysis of an improved LuGre friction model for magnetorheological elastomer base isolator", *Meccanica*, **50**(11), 2691-2707.
Yu, Y., Li, Y. and Li, J. (2015a), "Parameter identification of a novel strain stiffening model for magnetorheological elastomer base isolator utilizing enhanced particle swarm optimization", *J. Intel. Mat. Syst. Struct.*, **26**(18), 2446-2462.